bioRxiv preprint doi: https://doi.org/10.1101/826370; this version posted November 18, 2019. The copyright holder for this preprint (which was not certified by peer review) is the author/funder, who has granted bioRxiv a license to display the preprint in perpetuity. It is made available under aCC-BY-NC-ND 4.0 International license.

Histone methyltransferase DOT1L controls state-specific identity during B cell differentiation

Muhammad Assad Aslam[1,2]*, Mir Farshid Alemdehy[1]*, Eliza Mari Kwesi-Maliepaard[3,*], Marieta Caganova[4], Iris N. Pardieck[5], Teun van den Brand[3,6], Fitriari Izzatunnisa Muhaimin[1], Tibor van Welsem[3], Iris de Rink[7], Ji-Ying Song[8], Elzo de Wit[3,6], Ramon Arens[5], Klaus Rajewsky[4], Heinz Jacobs[1,#], and Fred van Leeuwen[3,9,#]

[1]Division of Tumor Biology and Immunology, Netherlands Cancer Institute, 1066CX Amsterdam, The Netherlands

[2]Institute of Molecular Biology and Biotechnology, Bahauddin Zakariya University, 60800 Multan, Pakistan

[3]Division of Gene Regulation, Netherlands Cancer Institute, 1066CX Amsterdam, The Netherlands

[4]Max-Delbrück-Center for Molecular Medicine, 13125 Berlin, Germany

[5]Immunohematology and Blood Transfusion, Leiden University Medical Center, 2333 ZA Leiden, The Netherlands

[6]Division of Gene Regulation, Netherlands Cancer Institute, 1066CX Amsterdam, and Oncode Institute The Netherlands

[7]Genome Core Facility, Netherlands Cancer Institute, 1066CX Amsterdam, The Netherlands

[8]Division of Experimental Animal Pathology, Netherlands Cancer Institute, 1066CX Amsterdam, The Netherlands

[9]Department of Medical Biology, Amsterdam UMC, location AMC, UvA, 1105 AZ Amsterdam, The Netherlands

* These authors contributed equally this work

[#] Equal contribution and corresponding authors

fred.v.leeuwen@nki.nl; h.jacobs@nki.nl

Lead Contact: Heinz Jacobs

bioRxiv preprint doi: https://doi.org/10.1101/826370; this version posted November 18, 2019. The copyright holder for this preprint (which was not certified by peer review) is the author/funder, who has granted bioRxiv a license to display the preprint in perpetuity. It is made available under aCC-BY-NC-ND 4.0 International license.

Abstract

Development of naïve peripheral B cells into terminally differentiated plasma cells is a highly controlled process guided by epigenetic mechanisms. Here we identified a central role for the histone H3K79 methyltransferase DOT1L in controlling B cell development. Upon deletion of *Dot1L* early in the B-cell lineage, naïve and activated B cells prematurely acquired plasma cell features and failed to establish germinal centers (GC) and normal humoral immune responses *in vivo*. Transcriptome analyses revealed that DOT1L promotes expression of oncogenic, pro-proliferative and pro-GC transcription factors. Simultaneously, DOT1L indirectly promotes repression of anti-proliferative targets of the Polycomb Repressor Complex 2. Our findings show that DOT1L fine tunes the transcriptional and epigenetic landscape in B cells. In doing so it establishes a critical epigenetic barrier warranting B cell naivety and prohibiting their premature differentiation towards plasma cells.

Key words

Epigenetics, B cell differentiation, DOT1L, H3K79 methylation, Germinal Center B cell, Plasma cell

Running title: DOT1L: A key regulator of B cell development

bioRxiv preprint doi: https://doi.org/10.1101/826370; this version posted November 18, 2019. The copyright holder for this preprint (which was not certified by peer review) is the author/funder, who has granted bioRxiv a license to display the preprint in perpetuity. It is made available under aCC-BY-NC-ND 4.0 International license.

INTRODUCTION

Epigenetic mechanisms warrant that one genome can upkeep multiple cellular identities[1]. This is directed by external and internal signals that instruct cells in adapting specific identities and functions[2]. These signals lead to the establishment of stage- and tissue-specific patterns of a variety of epigenetic alterations, including post-translational histone modifications that together with transcriptional regulators determine the gene expression program of a cell[3-6]. To maintain cellular identity and function, it is essential that specific writer-, reader-, and eraser-proteins ensure that epigenetic marks can be timely installed, interpreted, and eventually de-installed[7,8]. As a result, the epigenome is dynamic and permits cells to acquire new identities and functions.

We previously identified DOT1L as a conserved epigenetic writer that catalyzes mono-, di-, or tri-methylation of lysine 79 of histone H3 (H3K79me)[9,10], that resides away from histone tails containing a plethora of other modifications[11]. DOT1L-mediated H3K79me is associated with active transcription but its function in gene expression remains unclear[12-14]. DOT1L has gained wide attention as a specific drug target in the treatment of Mixed Lineage Leukemia (MLL) characterized by rearrangements of the *MLL* gene. In MLL cells, MLL-fusion proteins recruit DOT1L, leading to hypermethylation of H3K79 and increased expression of MLL-target genes, thereby introducing a druggable dependency on DOT1L activity[15-21]. In addition, we recently observed a similar dependency in a mouse model of thymic lymphoma caused by loss of the histone deacetylase HDAC1[22]. While DOT1L is emerging as an appealing drug target, the role of DOT1L in gene regulation during normal lymphocyte development is not known.

Analysis of publicly-available RNA-sequencing data shows that *Dot1L* expression is regulated during B cell development (see below). B lymphocytes are key players of the adaptive immune system. An active humoral immune response is characterized by the activation of clonally selected, antigen-primed B cells within secondary lymphoid organs. This results in the formation of a specific micro-environment, known as the germinal center (GC) [23,24]. Rapidly proliferating GC B cells pass through the process of somatic hypermutation that lays the molecular basis of antibody affinity maturation[25-29]. Ultimately, B cells selected on the basis of antibody affinity may

bioRxiv preprint doi: https://doi.org/10.1101/826370; this version posted November 18, 2019. The copyright holder for this preprint (which was not certified by peer review) is the author/funder, who has granted bioRxiv a license to display the preprint in perpetuity. It is made available under aCC-BY-NC-ND 4.0 International license.

differentiate either into memory B cells to establish long-term immunological memory or via a plasma blast stage into terminally differentiated, antibody secreting plasma cells.

Development and functionality of B lymphocytes is associated with dynamic changes in the epigenetic landscape[30]. Recent studies indicate that specific alterations in B cell function and identity are intimately linked with well-established histone modifications such H3K4 trimethylation (H3K4me3) related with active gene promoters[31,32], and H3K27me3 associated with gene repression[33]. Furthermore, the H3K27 methyltransferase EZH2, the catalytic component of the Polycomb repressor complex 2 (PRC2) has been shown to have an essential role in establishing GC B cells[34].

Here we determined the role of the H3K79 methyltransferase DOT1L in normal murine B cell development by deleting *Dot1L* early in the B cell lineage and investigating specific dependencies of B lineage cells on DOT1L. Our findings show that DOT1L fine-tunes the core transcriptional and epigenetic landscape of B cells and in doing so establishes a critical epigenetic barrier towards terminal plasma cell differentiation.

bioRxiv preprint doi: https://doi.org/10.1101/826370; this version posted November 18, 2019. The copyright holder for this preprint (which was not certified by peer review) is the author/funder, who has granted bioRxiv a license to display the preprint in perpetuity. It is made available under aCC-BY-NC-ND 4.0 International license.

RESULTS

Effective deletion of *Dot1L* in B-cell lineage cells

Given the DOT1L-dependencies in leukemia[16,17,35,36] and lymphoma[22], we quantified the expression of *Dot1L* during normal B cell development using publicly available data[37]. In doing so, we observed that *Dot1L* is transcriptionally regulated in B cell subsets and highly expressed in GC B cells (Fig. 1a). To determine the relevance of this regulation in controlling the development and differentiation of B lineage cells, we inactivated *Dot1L* during early B cell development by crossing the *Mb1*-Cre knock-in allele into a *Dot1L*$^{fl/fl}$ background. DOT1L is the sole enzyme responsible for H3K79me; knock-out of *Dot1L* has been shown to lead to complete loss of H3K79me[13,22,38,39]. However, loss of H3K79 methylation requires dilution of modified histones by replication-dependent and –independent mechanisms of histone exchange[40-42]. *Dot1L* was specifically and efficiently deleted in B cells, as confirmed by intracellular staining for H3K79me2 in proB, preB, immature B cells, and mature B cells. While some proB cells retained H3K79me2, preB cells and all stages beyond, lacked detectable levels of H3K79me2 (Fig. 1b). As a control, the methylation mark remained unchanged between DOT1L-proficient and -deficient mature T cells (Fig. 1B). We refer to *Mb1*-Cre$^{+/-}$;*Dot1L*$^{fl/fl}$ and *Mb1*-Cre$^{+/-}$;*Dot1L*$^{wt/wt}$ B cells as *Dot1L* KO and WT cells, respectively.

DOT1L-deficiency inhibits development of preB cells

To study the impact of *Dot1L* ablation on the development of B cells in the bone marrow, we determined the cellularity of specific developmental subsets in the DOT1L proficient and deficient settings. Early ablation of *Dot1L* resulted in an overall 1.6-fold reduction of bone marrow B lineage cells. This reduction appeared to be caused primarily by an early differentiation block at the proB to preB cell stage, preB cell were reduced 1.8-fold in the Dot1L KO as compared to WT and proB cells were increased by 2.0-fold. In line with this partial developmental inhibition, the cellularity of all subsequent stages of development including immature B and mature B cells were significantly reduced in the bone marrow (Fig. 1c and see Supplementary Fig. 1a). Reduced preB cells could be a result of impaired VDJ recombination in absence of DOT1L-dependent pro-recombinogenic H3K79me marks[43,44], an observation that requires further investigation. Regardless of this partial developmental block, B cells could mature in the absence of DOT1L providing a H3K79-methylation free system to study B cells differentiation. Given the high

bioRxiv preprint doi: https://doi.org/10.1101/826370; this version posted November 18, 2019. The copyright holder for this preprint (which was not certified by peer review) is the author/funder, who has granted bioRxiv a license to display the preprint in perpetuity. It is made available under aCC-BY-NC-ND 4.0 International license.

expression of *Dot1L* in GC B cells, we decided to investigate the impact of DOT1L ablation on the development of GC B cells.

Lack of DOT1L prohibits differentiation of germinal-center B cells

In the spleen of *Mb1*-Cre$^{+/-}$;*Dot1L*$^{fl/fl}$ mice, B cell cellularity decreased 3.5-fold while T cell numbers remained unaffected, resulting in a 2.0-fold decreased overall cellularity (Fig. 2a and 2b). Among the various peripheral B cell subsets, the strongest reduction was found in marginal zone B cells and GC B cells to the extent that they were nearly absent (Fig. 2c-i and see Supplementary Fig. 1b). The reduction of GC B cells was of particular interest given the high levels of *Dot1L* mRNA expression in this subset (Fig. 1a and 2i), and strongly suggested that the formation of germinal centers critically depends on DOT1L. Indeed, *in situ* histological analyses also revealed the absence of GCs in the spleen of Dot1L KO mice (Fig. 2j and 2k). Similarly, lack of DOT1L resulted in a marked reduction of GC B cells in Peyer's patches (see Supplementary Fig. 2).

Dot1L* deletion impairs class switch recombination and proliferation *in vitro

An important feature of humoral immunity is the ability of B cells to undergo class switch recombination (CSR). To investigate the role of DOT1L in CSR, naïve B cells were isolated from the spleen and stimulated *in vitro* with LPS alone or in combination with IL-4, to induce switching to IgG3 or IgG1, respectively. Compared to *Dot1L*-proficient B cells, the lack of *Dot1L* was associated with a strong impairment in switching to both IgG3 and IgG1 (Fig. 3a, 3b, see Supplementary Fig. 3a and see Supplementary Fig. 3b). Similar observations were made using the T-cell dependent mimetic anti-CD40 and IL-4 as stimuli (Fig. 3c and see Supplementary Fig. 3c). RNA-Seq analysis of KO and WT B cells activated with LPS and IL-4 argued against a potential failure of KO B cells in expressing specific components of the CSR machinery (see Supplementary Table 1). Of note, the proliferative response of KO B cells was also strongly impaired upon CD40+IL-4 *in vitro* stimulation, as revealed by tracing the dilution of a fluorescence label (Fig. 3d). The virtual absence of GC B cells, impaired proliferative response, and the reduced CSR potential of DOT1L-deficient B cells implicated a severe defect of *Mb1*-Cre$^{+/-}$;*Dot1L*$^{fl/fl}$ mice in establishing effective humoral immunity.

bioRxiv preprint doi: https://doi.org/10.1101/826370; this version posted November 18, 2019. The copyright holder for this preprint (which was not certified by peer review) is the author/funder, who has granted bioRxiv a license to display the preprint in perpetuity. It is made available under aCC-BY-NC-ND 4.0 International license.

DOT1L-deficient B cells fail to mount efficient immune responses but acquire premature plasma cell features

To determine the immune responsiveness of *Dot1L*-deficient B cells, *Mb1*-Cre$^{+/-}$;*Dot1L*$^{fl/fl}$ and *Mb1*-Cre$^{+/-}$;*Dot1L*$^{wt/wt}$ mice were challenged with an acute lymphocytic choriomeningitis virus (LCMV) infection. During the LCMV infection *Dot1L*-deficient B cells failed to establish GC B cells but interestingly acquired plasma cell markers (Fig. 4a and 4b). However, despite an increased plasma cell formation, these mice failed to mount normal IgM serum titers against LCMV (Fig. 4c). The failure to establish GCs in response to LCMV appeared in line with the very low LCMV-specific IgG serum titers (Fig. 4c). Independently, the inability of *Mb1*-Cre$^{+/-}$;*Dot1L*$^{fl/fl}$ mice to mount efficient antibody responses to T-cell dependent antigen was confirmed using the 4-hydroxy-3-nitrophenylacetyl conjugated to chicken gamma globulin (NP-CGG) in alum as immunogen (Fig. 4d). These data suggest that a DOT1L deficiency in the B cell lineage prohibits GC B cell differentiation and favors differentiation towards plasma cells. Remarkably, *in vitro* activation of naïve DOT1L-KO B cells with LPS and IL-4 confirmed a significantly increased plasma cell differentiation as compared to DOT1L-WT (see Supplementary Fig. 4a). However, these cells failed to downregulate B220 (see Supplementary Fig. 4b), which is considered as a hallmark of post-mitotic plasma cells. This might indicate an incomplete_differentiation of *Dot1L*-KO plasma cells[45]. Apparently, in the absence of H3K79 methylation naïve B cells skip the GC stage and start to gain prematurely plasma cell features.

DOT1L supports a pro-proliferative, MYC-high GC stage and prohibits premature plasma cell differentiation

To unravel the underlying molecular mechanisms that prohibit *Dot1L*-KO GC B cell differentiation and stimulate plasma cell formation we opted for an unbiased approach and performed RNA-Seq analyses of naïve and *in vitro* activated (LPS and IL-4) B cells under *Dot1L*-proficient and -deficient conditions. Among the differentially-expressed genes, the genes encoding the pro-GC transcription factor BACH2 and the pro-proliferative transcription factor MYC[28,46,47] were downregulated in activated DOT1L-deficient B cells; at the same time the pan-plasma cell transcription factor *Prdm1* encoding BLIMP1[48,49] was found upregulated (Fig. 5a and 5b). This agrees with the observed absence of GC B cells and increased plasma cell formation in KO cells. In addition, analysis of a published plasma-cell gene signature [37], revealed that the transcriptome of activated *Dot1L*-deficient B cells was indeed strongly enriched for plasma-cell associated transcripts (Fig. 5c). Simultaneously, MYC-target gene transcripts were strongly reduced (Fig. 5d). Together, these observations indicate that DOT1L-mediated H3K79 methylation licenses

bioRxiv preprint doi: https://doi.org/10.1101/826370; this version posted November 18, 2019. The copyright holder for this preprint (which was not certified by peer review) is the author/funder, who has granted bioRxiv a license to display the preprint in perpetuity. It is made available under aCC-BY-NC-ND 4.0 International license.

a transient entrance into a pro-proliferative, MYC-high GC stage and is required to prevent premature differentiation of activated B cells towards non-proliferative terminally differentiated plasma cells. Interestingly, transcriptomic data from *ex vivo* isolated naïve *Dot1L*-deficient B cells revealed some enrichment for B cell activation and plasma-cell associated genes, suggesting that already antigen-inexperienced B cells are pre-activated and prematurely differentiated in the absence of DOT1L (see Supplementary Fig. 5a).

DOT1L-mediated H3K79 methylation is associated with gene activity in B cells

To link the phenotypes of loss of DOT1L to its role as an epigenetic regulator in B cells, we generated genome-wide maps of DOT1L-mediated H3K79me2 in naïve and activated WT B cells by ChIP-Seq. We chose to analyze the H3K79me2 mark because it is known to mark the region downstream of the transcriptional start site of transcribed genes and positively correlate with gene activity[12,13,50,51]. While H3K79me1 shows the same trends, it has a broader distribution, and H3K79me3 is detectable only at limited levels[12,22,51]. Surprisingly, more than 83 percent of the differentially expressed genes was found upregulated in the absence of DOT1L; only a small subset was downregulated (Fig. 5a and see Supplementary Fig. 5b). Furthermore, the upregulation was biased towards more lowly expressed genes. The observed upregulation of genes in *Dot1L*-KO B cells was unexpected given the fact that H3K79me2 generally correlates with transcriptional activity[12,14,20,50,52-55]. However, repressive functions of DOT1L have been proposed as well[56-59]. Comparing H3K79me2 ChIP values in WT cells with the gene expression changes caused by loss of DOT1L revealed that the genes upregulated in *Dot1L*-KO B cells were mostly hypomethylated in WT cells, indicating that they are likely indirectly affected by the loss of DOT1L (Fig. 6a and 6b). In contrast, genes downregulated in *Dot1L*-KO B cells were generally highly expressed and H3K79 methylated in WT B cells, indicating that this gene set harbors the genes directly dependent on DOT1L. These findings show that DOT1L-mediated H3K79me2 is a mark of many active genes, but suggest that only a small fraction of these genes requires H3K79me2 for maintenance of gene expression, since only a subset of the active genes was downregulated in *Dot1L* KO.

DOT1L indirectly supports repression of PRC2 target genes

bioRxiv preprint doi: https://doi.org/10.1101/826370; this version posted November 18, 2019. The copyright holder for this preprint (which was not certified by peer review) is the author/funder, who has granted bioRxiv a license to display the preprint in perpetuity. It is made available under aCC-BY-NC-ND 4.0 International license.

The large number of genes found upregulated in *Dot1L*-KO B cells indicated that DOT1L positively regulates the expression of a transcriptional repressor whose target genes are derepressed in absence of DOT1L. To identify such candidate repressors, we investigated the relatively small fraction of genes downregulated in naïve *Dot1L*-KO B cells. Unbiased identification of upstream transcriptional regulators by Ingenuity pathway analyses (IPA) pointed towards nine potential regulators (Table 1). To further narrow down the list, we filtered for genes that are (i) H3K79-dimethylated by DOT1L, (ii) encode transcriptional repressors, and (iii) play a role in B cell differentiation/proliferation and GC formation. This led to the identification of the histone H3K27 methyltransferase EZH2 as a prime candidate (Table 1). We verified that *Ezh2* expression was reduced in DOT1L KO B cells (Fig. 6c) and that the gene is H3K79-dimethylated in WT cells (Fig. 6d), indicating that the expression of *Ezh2* might be directly supported by DOT1L activity (Fig. 6c and 6d). Of note, the expression of *Ezh2* and *Dot1L* was found co-regulated in B cell subsets (Fig. 6e).

We next investigated the physiological relevance of the connection between DOT1L and EZH2. First, *Ezh2*-KO and *Dot1L*-KO B cells have overlapping phenotypes[34,60-63, 85]. Second, we took advantage of publicly available RNA-Seq data [61] from *Ezh2* -KO plasma cells to identify genes that require EZH2 for being repressed (see Supplementary Fig. 6a). Using this as a signature of EZH2-dependent genes, we found that many of the genes de-repressed in *Ezh2*-KO cells were also found de-repressed in activated *Dot1L*-KO B cells (see Supplementary Fig. 6b). Surprisingly, many of these genes were found de-repressed also in naïve *Dot1L*-KO B cells, suggesting that lack of DOT1L renders these cells prematurely differentiated (see Supplementary Fig. 6b). As a specific example, we checked the expression of a known PRC2-target gene *Cdkn1a* (*p21*)[62,64,65], and found that it was upregulated in activated *Dot1L*-KO B cells (Fig. 6c). Third, we analyzed the level of H3K27me3 and H3K79me2 in the set of genes that was de-repressed in *Dot1L* KO using our H3K79me2 ChIP-Seq data and publicly available H3K27me3 ChIP-Seq data from naïve B cells[66]. The analysis revealed that this gene set was enriched for H3K27me3 in WT cells compared to expression-matched non-differentially expressed genes (Fig. 6f). Together, these findings suggest that in B cells, DOT1L supports the repression of PRC2 target genes, thus uncovering a previously unknown connection between two conserved histone methyltransferases associated with activation and repression, respectively.

bioRxiv preprint doi: https://doi.org/10.1101/826370; this version posted November 18, 2019. The copyright holder for this preprint (which was not certified by peer review) is the author/funder, who has granted bioRxiv a license to display the preprint in perpetuity. It is made available under aCC-BY-NC-ND 4.0 International license.

DISCUSSION

B lymphocytes are key cellular components of the adaptive immune system and their functional deregulation is associated with immune deficiencies and autoimmunity[67,68]. Several well-coordinated processes during B cell differentiation coincide with specific adaptations of the epigenome[69-71]. Given the critical contribution of B cells to the immune system, it is important to understand the molecular mechanisms underlying their epigenetic programming. We observed that the H3K79 methyltransferase DOT1L is regulated in B cell development and has a central role in B cell physiology.

GC B cell differentiation was found to be critically dependent on DOT1L activity. Among mature B cells, GC B cells express the highest levels of *Dot1L* and they were strongly reduced in *Dot1L*-KO mice. Upon activation *in vitro* or immune challenge *in vivo, Dot1L*-KO B cells failed to proliferate, differentiate into GC B cells, and establish effective immune responses. Rather, we found indications of accelerated plasma cell differentiation in *Dot1L*-KO mice, both *in vitro* and *in vivo*. RNA-Seq data generated from naïve and *in vitro* activated *Dot1L*-KO and WT B cells confirmed the strong enrichment of genes associated with plasma cell differentiation among the genes up-regulated in *Dot1L* KO. The data also revealed that DOT1L supports MYC activity, which B cells need to differentiate effectively into pro-proliferative GC B cells[28]. Recent studies have also shown that inhibition of DOT1L leads to reduced *Myc* expression in multiple myeloma[72] and in MYC-driven B cell lymphoma[73]. Furthermore, in neuroblastoma H3K79me2 methylation has been shown to be a strict prerequisite for Myc-induced transcriptional activation, indicating a mutual interaction between DOT1L and MYC[74]. In addition to the crucial role in GC formation we also identify DOT1L as a critical factor in maintaining MZ B cells. Exploring the strong reduction of MZ B cells upon loss of *Dot1L* should provide additional insights regarding the contribution of DOT1L in orchestrating normal B cell physiology.

In addition to supporting MYC activity, our findings show that DOT1L supports the repression of target genes of PRC2. The observation that *Ezh2* is normally H3K79-dimethylated and downregulated in *Dot1L*-KO B cells, and that *Dot1L* and *Ezh2* are co-regulated in B cells indicates that DOT1L may promote repression of PRC2 targets by maintaining expression of *Ezh2*. A direct stimulatory effect of H3K79me on H3K27me3 synthesis is not likely to be

bioRxiv preprint doi: https://doi.org/10.1101/826370; this version posted November 18, 2019. The copyright holder for this preprint (which was not certified by peer review) is the author/funder, who has granted bioRxiv a license to display the preprint in perpetuity. It is made available under aCC-BY-NC-ND 4.0 International license.

involved since the modifications occur in distinct locations in the genome and are associated with opposite transcriptional states. Finally, besides MYC and PRC2, additional factors controlled by DOT1L may impart its effect on B cells. For example, it will be interesting to determine the role of other candidate transcriptional regulators regulated by DOT1L (Table 1).

Our finding regarding the central role of DOT1L in lymphocyte biology is also supported by our study in the T cell lineage (Kwesi-Maliepaard et al.). First, in both lineages, DOT1L is required to establish an epigenetic barrier in naïve lymphocytes to prohibit their premature differentiation. Second, in spite of gaining many advanced features related to differentiation, both lineages displayed a compromised immune response. Third, in B and T cells DOT1L promotes repression of PRC2 targets normally associated with differentiation.

In summary, in lymphocytes, DOT1L has a central role in maintaining a naive lymphocyte pool and guiding dynamic epigenetic states controlling differentiation and ensuring functional immune responses.

bioRxiv preprint doi: https://doi.org/10.1101/826370; this version posted November 18, 2019. The copyright holder for this preprint (which was not certified by peer review) is the author/funder, who has granted bioRxiv a license to display the preprint in perpetuity. It is made available under aCC-BY-NC-ND 4.0 International license.

Methods

Mice

Mb1-Cre$^{+/-}$;*Dot1L*$^{fl/fl}$ mice were derived by crossing the Dot1Ltm1a(KOMP)Wtsi line - generated by the Wellcome Trust Sanger Institute (WTSI) and obtained from the KOMP Repository (www.komp.org) - with the MB1-Cre strain kindly provided by M. Reth[87]. Mice from this newly created *Mb1*-Cre$^{+/-}$;*Dot1L* strain were maintained under specific pathogen free (SPF) conditions at the animal laboratory facility of the Netherlands Cancer Institute (NKI; Amsterdam, Netherlands). Mice used for experiments were between 6-8 weeks old and of both genders. All experiments were approved by the Animal Ethics Committee of the NKI and performed in accordance with the Dutch Experiments on Animals Act and the Council of Europe.

Genotyping PCR

Mice were genotyped for *Dot1L* using the forward primer (Dot1L: FWD, GCAAGCCTACAGCCTTCATC) and reverse primer 1 (Dot1L:REV1, CACCGGATAGTCTCAATAATCTCA) to identify WT allele; *Dot1L*^{wt} (642 Bps) while the floxed allele; *Dot1L*^{fl} (1017 Bps) was identified by using Dot1L: FWD and reverse primer 2 (Dot1L:REV2, GAACCACAGGATGCTTCAG). WT allele (418 Bps) for *Mb1* was detected by using forward primer (Mb1-FWD1: CTGCGGGTAGAAGGGGGTC) and reverse primer (Mb1-REV1: CCTTGCGAGGTCAGGGAGCC) while *Cre* (219 Bps) was detected by using forward primer (Mb1-FWD2: GTGCAAGCTGAACAACAGGA) and reverse primer (Mb1-REV2: AAGGAGAATGTGGATGCTGG).

Flow cytometry

Single cell suspensions were made from bone marrow, spleen and Peyer's patches. Bone marrow, spleen and blood samples were subjected to erythrocyte lysis. Distinct cellular populations were identified using combination of fluor-conjugated antibodies against surface markers (Table 2). Cells were stained with fluorescently labeled antibodies (Table 3). For intracellular staining cells were fixed and permeabilized using the Transcription Factor Buffer kit (Becton Dickinson, BD). Antibodies for intracellular staining were diluted in Perm/Wash buffer. For H3K79me2 staining, cells were first stained with surface markers and fixed and permeabilized as described before.

bioRxiv preprint doi: https://doi.org/10.1101/826370; this version posted November 18, 2019. The copyright holder for this preprint (which was not certified by peer review) is the author/funder, who has granted bioRxiv a license to display the preprint in perpetuity. It is made available under aCC-BY-NC-ND 4.0 International license.

After fixation and permeabilization cells were washed with Perm/Wash containing 0.25% SDS. H3K79me2 specific antibody (Millipore) was diluted 1:200 into Perm/Wash + 0.25% SDS and cells were incubated for 30 min. Cells were washed with Perm/Wash and incubated with the secondary antibodies Donkey anti-Rabbit AF555 (Thermo Scientific) or Goat-anti-Rabbit AF488 (Invitrogen) 1:1000 in Perm/Wash. Flow cytometry was performed using the LSR Fortessa (BD Biosciences) and data were analyzed with FlowJo software (Tree Star inc.). Histograms were smoothed.

Immunization

Adult mice were inoculated intravenously with sub-lethal dose $2x10^5$ PFU (Plaque forming units) of lymphocytic choriomeningitis virus strain Armstrong. Serum was collected prior to immunization and 14 days post immune challenge. For NP-CGG immunization mice were injected intraperitoneally with 100 μg of alumprecipitated NP-CGG [(4-hydroxy-3-nitrophenyl) acetyl coupled to chicken γ–globulin, BIOSEARCH™ TECHNOLOGIES] in a 200 μl of NP-CGG alum solution. To determine the serum titers of NP-specific IgM and IgG1, mice were bled from the tail vein on day 0,7,14,21,28, and 35.

Class switch recombination and Proliferation

Single cells suspensions were prepared from the spleen of 6-8-week-old mice. Following erythrocyte lysis, naïve splenic B cells were enriched by the depletion of CD43 expressing cell using biotinylated anti-CD43 antibody (Clone S7, BD Biosciences), BD IMag Streptavidin Particles Plus and the IMag® system (BD Biosciences), as described by the manufacturer. To measure their proliferative capacity, naïve B cells were labeled for 10 min at 37°C with 5 μM Cell Trace Violet (CTV, Life Technologies, Invitrogen™) in IMDM medium containing 2% FCS,100 mM pen/strep and 100 mM β-mercaptoethanol. After washing, cells were cultured in complete IMDM medium (IMDM supplemented with 8% FCS, 100 mM pen/strep and 100 mM β-mercaptoethanol) at a density of 10^5 cells/well in 24 well plates. CSR to IgG3 and IgG1 was induced in T cell independent manner by exposure to 5 μg/ml of Lipopolysaccharide (Escherichia Coli LPS, 055:B5, Sigma) or LPS+rIL-4. rIL4 was used at a concentration of 10 ng/ml. Cells were exposed to anti-CD40 (1ug/ml, BD Clone HM40-3) and rIL-4 (10 ng/ml) to induce IgG1 switching in a T cell dependent

bioRxiv preprint doi: https://doi.org/10.1101/826370; this version posted November 18, 2019. The copyright holder for this preprint (which was not certified by peer review) is the author/funder, who has granted bioRxiv a license to display the preprint in perpetuity. It is made available under aCC-BY-NC-ND 4.0 International license.

manner. Four days later, the cells were harvested and stained with CD19, IgM, and IgG3 (LPS cultures) or IgG1 (LPS/rIL4 cultures or anti-CD40/rIL-4) to determine CSR frequency along with CTV dilution as an indicator of cell multiplication.

ELISA

LCMV-specific serum IgM and IgG levels were measured by ELISA. In short, Nunc-Immuno Maxisorp plates (Fisher Scientific) were coated overnight at 4°C with virus in bicarbonate buffer. Plates were subsequently incubated for 1h with blocking buffer (PBS/5% milk powder (Fluka Biochemika)). Sera from mice were diluted in PBS/1% milk powder and incubated for 1h at 37°C. Next, HRP-conjugated IgG and IgM antibodies (Southern Biotech) were diluted 1:4000 in PBS/1% milk powder and incubated 1h at 37°C. Plates were developed with TMB substrate (Sigma Aldrich), and the color reaction was stopped by the addition of 1 M H_2SO_4. Optical density was read at 450 nm (OD_{450}) using a Microplate reader (Model 680, Bio-Rad).

To quantify NP-specific serum antibodies, plates were coated with 2 µg/ml NP_{30}-BSA. Serum was added at a starting dilution of 1:100 followed by 3-fold serial dilutions and incubated at room temperature for 2 hours. Bound serum antibodies were detected with polyclonal biotinylated goat anti-mouse IgM or anti-IgG1 (Southern Biotech), streptavidin-alkaline phosphatase conjugate (Roche) and chromogenic substrate 4- nitrophenyl phosphate (Sigma). Purified monoclonal antibodies (B1-8µ and 18-1-16y1) were used as standards for quantification.

Lectin histochemistry

Lymphoid tissues such as spleens and lymph nodes were fixed in EAF (ethanol, acetic acid, formaldehyde, saline) for 24 hours and subsequently embedded in paraffin. 4 um-thick sections were stained with the lectin Peanut Agglutinin (PNA, Vector Laboratories) at 1:1500 dilution to reveal germinal centers. The sections were counterstained with hematoxyline.

Sorting and *in vitro* activation for RNA and ChIP-Seq

For RNA sequencing, cells were first depleted for CD43+ cells and either subjected to MACS sorting for CD19+ cells as naïve B cells or activated for two days with LPS and IL-4. Following activation, the cells were enriched for CD19+

bioRxiv preprint doi: https://doi.org/10.1101/826370; this version posted November 18, 2019. The copyright holder for this preprint (which was not certified by peer review) is the author/funder, who has granted bioRxiv a license to display the preprint in perpetuity. It is made available under aCC-BY-NC-ND 4.0 International license.

by MACS according to the manufacturer instructions. For ChIP-Seq, CD43- cells were either FACS sorted for CD19+ as naïve B cell pool or activated for three days with LPS and IL-4 and subjected to FACS sorting for CD19+ expression.

RNA-Seq sample preparation

MACS sorted CD19+ cells were resuspended in Trizol (Ambion Life Technologies) and total RNA was extracted according to the manufacturer's protocol. Quality and quantity of the total RNA was assessed by the 2100 Bioanalyzer using a Nano chip (Agilent). Only RNA samples having an RNA Integrity Number (RIN) > 8 were subjected to library generation.

RNA-Seq library preparation

Strand-specific cDNA libraries were generated using the TruSeq Stranded mRNA sample preparation kit (Illumina) according to the manufacturer's protocol. The libraries were analyzed for size and quantity of cDNAs on a 2100 Bioanalyzer using a DNA 7500 chip (Agilent), diluted and pooled in multiplex sequencing pools. The libraries were sequenced as 65 base single reads on a HiSeq2500 (Illumina).

RNA-Seq preprocessing

Strand-specific RNA reads (11-33 million reads per sample), 65 bp single-end, were aligned against the mouse reference genome (Ensembl build 38) using Tophat (version 2.1, bowtie version 1.1). Tophat was supplied with a Gene Transfer File (GTF, Ensembl version 77) and was supplied with the following parameters: `--prefilter-multihits –no-coverage-search –bowtie1 –library-type fr-firststrand`. In order to count the number of reads per gene, a custom script which is based on the same ideas as HTSeq-count has been used. A list of the total number of uniquely mapped reads for each gene that is present in the provided Gene Transfer Format (GTF) file was generated. Genes that have no expression across all samples within the dataset were removed. Analysis was restricted to genes that have least 2 counts per million (CPM) value in all samples in specific contrasts, to exclude very low abundance genes. Differential expression analysis was performed in R language (version 3.5.1) on only relevant samples using edgeR package and default arguments with the design set to either Dot1LKO status,

bioRxiv preprint doi: https://doi.org/10.1101/826370; this version posted November 18, 2019. The copyright holder for this preprint (which was not certified by peer review) is the author/funder, who has granted bioRxiv a license to display the preprint in perpetuity. It is made available under aCC-BY-NC-ND 4.0 International license.

Ezh2KO status or cell type. Genes were considered to be differentially expressed when the False discovery rate (FDR) was below 0.05 after the Benjamini-Hochberg multiple testing correction. Sets of differentially expressed genes in indicated conditions were called 'gene signatures. MA plots were generated after differential expression analysis carried by edgeR package[88,89]. Read counts were corrected for gene length based on the longest transcript of the gene followed by normalization for the library size and shown as transcript per million (TPM). Counts are shown as counts per million after trimmed mean of M-values (TMM) normalization using the edgeR R package. For analyses where we performed expression matching, we chose genes with an absolute log2 fold changes less than 0.1 and false discovery rate corrected p-values above 0.05 that were closest in mean expression to each of the genes being matched without replacement. The RNA-Seq datasets reported in this article have been deposited at the National Center for Biotechnology Information under the accession number GSE138909.

Gene set enrichment analysis (GSEA)

GSEA was carried out after differential expression analysis. Gene set enrichment was shown as barcode plot where the genes were ranked according to the log2 fold change between the compared conditions. Statistical significance for the enrichment of gene set was determined by Fast approximation to mroast (FRY) gene set test [90] from limma package and two-sided directional p value less than 0.05 was considered significant.

Functional enrichment analysis

Functional enrichment analysis was carried by 'g:GOST' tool with default arguments from 'g:Profiler2' package and performed in R language (version 3.5.1).

ChIP-Seq sample preparation

Sorted cells were centrifuged at 500 rcf. The pellet was resuspended in IMDM containing 2% FCS and formaldehyde (Sigma) was added to a final concentration of 1%. After 10 min incubation at RT glycine (final concentration 125 mM) was added and incubated for 5 min. Cells were washed twice with ice-cold PBS containing Complete, EDTA free, protein inhibitor cocktail (PIC) (Roche). Cross-linked cell pellets were stored at -80°C. Pellets were resuspended in cold Nuclei lysis buffer (50mM Tris-HCl pH 8.0, 10mM EDTA pH8.0, 1%SDS) + PIC and

bioRxiv preprint doi: https://doi.org/10.1101/826370; this version posted November 18, 2019. The copyright holder for this preprint (which was not certified by peer review) is the author/funder, who has granted bioRxiv a license to display the preprint in perpetuity. It is made available under aCC-BY-NC-ND 4.0 International license.

incubated for at least 10 min. Cells were sonicated with PICO to an average length of 200-500bp using 30s on/ 30s off for 3 min. After centrifugation at high speed debris was removed and 9x volume of ChIP dilution buffer (50mM Tris-HCl pH8, 0.167M NaCl, 1.1% Triton X-100, 0.11% sodium deoxycholate) + PIC and 5x volume of RIPA-150 (50mM Tris-HCl pH8, 0.15M NaCl, 1mM EDTA pH8, 0.1% SDS, 1% Triton X-100, 0.1% sodium deoxycholate) + PIC was added. Shearing efficiency was confirmed by reverse crosslinking the chromatin and checking the size on agarose gel. Chromatin was pre-cleared by adding ProteinG Dynabeads (Life Technologies) and rotation for 1 hour at 4°C. After the beads were removed 2µl H3K79me1, 2µl H3K79me2 (NL59, Merck Millipore) and 1µl H3K4me3 (ab8580, Abcam) were added and incubated overnight at 4°C. ProteinG Dynabeads were added to the IP and incubated for 3 hours at 4°C. Beads with bound immune complexes were subsequently washed with RIPA-150, 2 times RIPA-500 (50mM Tris-HCl pH8, 0.5M NaCl, 1mM EDTA pH8, 0.1% SDS, 1% Triton X-100, 0.1% sodium deoxycholate), 2 times RIPA-LiCl (50mM Tris-HCl pH8, 1mM EDTA pH8, 1% Nonidet P-40, 0.7% sodium deoxycholate, 0.5M LiCl2) and TE. Beads were resuspended in 150 µl Direct elution buffer (10mM Tris-HCl pH8, 0.3M NaCl, 5mM EDTA pH8, 0.5%SDS) and incubated overnight at 65°C and input samples were included. Supernatant was transferred to a new tube and 1µl RNase A (Sigma) and 3 µl ProtK (Sigma) were added per sample and incubated at 55°C for 1 hour. DNA was purified using Qiagen purification columns.

ChIP-Seq Library preparation

Library preparation was done using KAPA LTP Library preparation kit using the manufacturer's protocol with slight modifications. Briefly, after end-repair and A-tailing adaptor were ligated followed by Solid Phase Reversible Immobilization (SPRI) clean-up. Libraries were amplified by PCR and fragments between 250-450 bp were selected using AMPure XP beads (Beckman Coulter). The libraries were analyzed for size and quantity of DNAs on a 2100 Bioanalyzer using a High Sensitivity DNA kit (Agilent), diluted and pooled in multiplex sequencing pools. The libraries were sequenced as 65 base single reads on a HiSeq2500 (Illumina).

ChIP-Seq preprocessing

ChIP-Seq samples were mapped to mm10 (Ensembl GRCm38) using BWA-MEM with the option '-M'. Duplicate reads were removed using MarkDuplicates from the Picard toolset with `VALIDATION_STRINGENCY=LENIENT` and

bioRxiv preprint doi: https://doi.org/10.1101/826370; this version posted November 18, 2019. The copyright holder for this preprint (which was not certified by peer review) is the author/funder, who has granted bioRxiv a license to display the preprint in perpetuity. It is made available under aCC-BY-NC-ND 4.0 International license.

`REMOVE_DUPLICATES=true` as arguments. Bigwig tracks were generated from these bam files by using bamCoverage from deepTools using the following arguments: `-of bigwig –binsize 25 –normalizeUsing RPGC –ignoreForNormalization chrM –effectiveGenomeSize 2652783500`. Bigwig files were loaded into R using the `import.bw()` function from the rtracklayer R package for visualisation of heatmaps and genomic tracks. TSSs for heatmaps were taken from Ensembl GRCm38.77 gene models by taking the first base pair of the 5' UTR of transcripts. When such annotation was missing, the most 5' position of the first exon was taken. The ChIP-Seq datasets reported in this article have been deposited at the National Center for Biotechnology Information under the accession number GSE138906.

Statistics

Statistical analyses were performed using Prism 7 (Graphpad). Data are presented as mean ±SD except for Fig. 4D where it is presented as mean± SEM. The unpaired Student's t-test with two-tailed distributions was used to calculate the p-value. A p-value < 0.05 was considered statistically significant.

bioRxiv preprint doi: https://doi.org/10.1101/826370; this version posted November 18, 2019. The copyright holder for this preprint (which was not certified by peer review) is the author/funder, who has granted bioRxiv a license to display the preprint in perpetuity. It is made available under aCC-BY-NC-ND 4.0 International license.

Acknowledgements

We like to thank the core facilities of the NKI-AVL for their superb biotechnical and molecular help. We highly appreciate the support from Michael Reth in providing his *Mb1*-Cre mouse model system.

Funding

This work would not have been possible without the generous support kindly provided by the Netherlands Organization for Scientific Research (NWO-VICI-016.130.627 to FvL; ZonMW Top 91213018 to HJ; ZonMW Top91218022 to FvL and HJ) and the Dutch Cancer Society (NKI 2014-7232 to FvL and HJ). The funders had no role in study design, data collection and interpretation, or the decision to submit the work for publication.

Author contributions

Conception and design, M.A.A, M.F.A., E.M.K-M., F.v.L., and H.J.

Acquisition of data, M.A.A., M.F.A., E.M.K-M., M.C., I.N.P., T.v.W., J-Y.S., and F.I.M.

Analysis and interpretation of data, M.A.A, M.F.A., E.M.K-M., R.A., E.d.W., K.R., F.v.L., and H.J.

Bioinformatics Analysis, M.A.A, T. v.d. B., M.F.A, E.d.W, and I.d.R.

Writing of the manuscript, M.A.A., M.F.A., E.M.K-M., F.v.L. and H.J.

bioRxiv preprint doi: https://doi.org/10.1101/826370; this version posted November 18, 2019. The copyright holder for this preprint (which was not certified by peer review) is the author/funder, who has granted bioRxiv a license to display the preprint in perpetuity. It is made available under aCC-BY-NC-ND 4.0 International license.

REFERENCES

1. Barrero, M.J., Boue, S. & Izpisua Belmonte, J.C. Epigenetic mechanisms that regulate cell identity. *Cell Stem Cell* **7**, 565-570 (2010).
2. Cavalli, G. & Heard, E. Advances in epigenetics link genetics to the environment and disease. *Nature* **571**, 489-499 (2019).
3. Arrowsmith, C.H., Bountra, C., Fish, P.V., Lee, K. & Schapira, M. Epigenetic protein families: a new frontier for drug discovery. *Nat. Rev Drug Discov* **11**, 384-400 (2012).
4. Etchegaray, J.-P. & Mostoslavsky, R. Interplay between Metabolism and Epigenetics: A Nuclear Adaptation to Environmental Changes. *Mol. Cell* **62**, 695-711 (2016).
5. Feinberg, A.P., Koldobskiy, M.A. & Göndör, A. Disease mechanisms: Epigenetic modulators, modifiers and mediators in cancer aetiology and progression. *Nat. Rev. Genet.* **17**, 284-299 (2016).
6. Laugesen, A. & Helin, K. Chromatin Repressive Complexes in Stem Cells, Development, and Cancer. *Cell Stem Cell* **14**, 735-751 (2014).
7. Hyun, K., Jeon, J., Park, K. & Kim, J. Writing, erasing and reading histone lysine methylations. *Exp Mol Med* **49**, e324 (2017).
8. Kouzarides, T. Chromatin modifications and their function. *Cell* **128**, 693-705 (2007).
9. van Leeuwen, F., Gafken, P.R. & Gottschling, D.E. Dot1p modulates silencing in yeast by methylation of the nucleosome core. *Cell* **109**, 745-756 (2002).
10. Frederiks, F. et al. Nonprocessive methylation by Dot1 leads to functional redundancy of histone H3K79 methylation states. *Nat. Struct. Mol. Biol.* **15**, 550-557 (2008).
11. Vlaming, H. et al. Flexibility in crosstalk between H2B ubiquitination and H3 methylation in vivo. *EMBO Rep.* **15**, 1077-1084 (2014).
12. Steger, D.J. et al. DOT1L/KMT4 recruitment and H3K79 methylation are ubiquitously coupled with gene transcription in mammalian cells. *Mol. Cell. Biol.* **28**, 2825-2839 (2008).
13. Vlaming, H. & van Leeuwen, F. The upstreams and downstreams of H3K79 methylation by DOT1L. *Chromosoma* **125**, 593-605 (2016).
14. Wood, K., Tellier, M. & Murphy, S. DOT1L and H3K79 Methylation in Transcription and Genomic Stability. *Biomolecules* **8** (2018).
15. McLean, C.M., Karemaker, I.D. & van Leeuwen, F. The emerging roles of DOT1L in leukemia and normal development. *Leukemia* **28**, 2131-2138 (2014).
16. Wang, X., Chen, C.W. & Armstrong, S.A. The role of DOT1L in the maintenance of leukemia gene expression. *Curr Opin Genet Dev* **36**, 68-72 (2016).
17. Stein, E.M. et al. The DOT1L inhibitor pinometostat reduces H3K79 methylation and has modest clinical activity in adult acute leukemia. *Blood* **131**, 2661-2669 (2018).
18. Chen, C.-W. et al. DOT1L inhibits SIRT1-mediated epigenetic silencing to maintain leukemic gene expression in MLL-rearranged leukemia. *Nat Med* **21**, 335-343 (2015).
19. Daigle, S.R. et al. Selective killing of mixed lineage leukemia cells by a potent small-molecule DOT1L inhibitor. *Cancer Cell* **20**, 53-65 (2011).
20. Bernt, K.M. et al. MLL-rearranged leukemia is dependent on aberrant H3K79 methylation by DOT1L. *Cancer Cell* **20**, 66-78 (2011).
21. Okada, Y. et al. Leukaemic transformation by CALM–AF10 involves upregulation of Hoxa5 by hDOT1L. *Nat. Cell Biol.* **8**, 1017-1024 (2006).
22. Vlaming, H. et al. Conserved crosstalk between histone deacetylation and H3K79 methylation generates DOT1L-dose dependency in HDAC1-deficient thymic lymphoma. *EMBO J.* **38**, e101564 (2019).
23. MacLennan, I.C. Germinal centers. *Annu Rev Immunol* **12**, 117-139 (1994).
24. MacLennan, I.C. Germinal centers still hold secrets. *Immunity* **22**, 656-657 (2005).
25. Di Noia, J.M. & Neuberger, M.S. Molecular mechanisms of antibody somatic hypermutation. *Annu. Rev. Biochem.* **76**, 1-22 (2007).
26. Odegard, V.H. & Schatz, D.G. Targeting of somatic hypermutation. *Nat Rev Immunol* **6**, 573-583 (2006).
27. Pilzecker, B. & Jacobs, H. Mutating for Good: DNA Damage Responses During Somatic Hypermutation. *Front Immunol* **10**, 438 (2019).
28. Calado, D.P. et al. The cell-cycle regulator c-Myc is essential for the formation and maintenance of germinal centers. *Nat Immunol* **13**, 1092-1100 (2012).
29. Victora, G.D. & Nussenzweig, M.C. Germinal centers. *Annu Rev Immunol* **30**, 429-457 (2012).
30. Martin-Subero, J.I. & Oakes, C.C. Charting the dynamic epigenome during B-cell development. *Semin Cancer Biol* **51**, 139-148 (2018).

bioRxiv preprint doi: https://doi.org/10.1101/826370; this version posted November 18, 2019. The copyright holder for this preprint (which was not certified by peer review) is the author/funder, who has granted bioRxiv a license to display the preprint in perpetuity. It is made available under aCC-BY-NC-ND 4.0 International license.

31. Zhang, J. et al. Disruption of KMT2D perturbs germinal center B cell development and promotes lymphomagenesis. *Nat Med* **21**, 1190-1198 (2015).
32. Li, B., Carey, M. & Workman, J.L. The role of chromatin during transcription. *Cell* **128**, 707-719 (2007).
33. Beguelin, W. et al. EZH2 and BCL6 Cooperate to Assemble CBX8-BCOR Complex to Repress Bivalent Promoters, Mediate Germinal Center Formation and Lymphomagenesis. *Cancer Cell* **30**, 197-213 (2016).
34. Béguelin, W. et al. EZH2 Is Required for Germinal Center Formation and Somatic EZH2 Mutations Promote Lymphoid Transformation. *Cancer Cell* **23**, 677-692 (2013).
35. Daigle, S.R. et al. Potent inhibition of DOT1L as treatment of MLL-fusion leukemia. *Blood* **122**, 1017-1025 (2013).
36. Shukla, N. et al. Final Report of Phase 1 Study of the DOT1L Inhibitor, Pinometostat (EPZ-5676), in Children with Relapsed or Refractory MLL-r Acute Leukemia. *Blood* **128** (2016).
37. Shi, W. et al. Transcriptional profiling of mouse B cell terminal differentiation defines a signature for antibody-secreting plasma cells. *Nat Immunol* **16**, 663-673 (2015).
38. Jones, B. et al. The histone H3K79 methyltransferase Dot1L is essential for mammalian development and heterochromatin structure. *PLoS Genet.* **4**, e1000190 (2008).
39. Feng, Y. et al. Early mammalian erythropoiesis requires the Dot1L methyltransferase. *Blood* **116**, 4483-4491 (2010).
40. Chory, E.J. et al. Nucleosome Turnover Regulates Histone Methylation Patterns over the Genome. *Mol. Cell* **73**, 1-12 (2018).
41. De Vos, D. et al. Progressive methylation of ageing histones by Dot1 functions as a timer. *EMBO Rep.* **12**, 956-962 (2011).
42. Radman-Livaja, M. et al. Patterns and mechanisms of ancestral histone protein inheritance in budding yeast. *PLoS Biol.* **9**, e1001075 (2011).
43. Xu, Z., Zan, H., Pone, E.J., Mai, T. & Casali, P. Immunoglobulin class-switch DNA recombination: induction, targeting and beyond. *Nat Rev Immunol* **12**, 517-531 (2012).
44. Deng, Z., Liu, H. & Liu, X. RAG1-mediated ubiquitylation of histone H3 is required for chromosomal V(D)J recombination. *Cell Res.* **25**, 181-192 (2015).
45. Kallies, A. et al. Plasma cell ontogeny defined by quantitative changes in blimp-1 expression. *J Exp Med* **200**, 967-977 (2004).
46. Muto, A. et al. The transcriptional programme of antibody class switching involves the repressor Bach2. *Nature* **429**, 566-571 (2004).
47. Muto, A. et al. Bach2 represses plasma cell gene regulatory network in B cells to promote antibody class switch. *EMBO J.* **29**, 4048-4061 (2010).
48. Martins, G. & Calame, K. Regulation and functions of Blimp-1 in T and B lymphocytes. *Annu Rev Immunol* **26**, 133-169 (2008).
49. Tellier, J. et al. Blimp-1 controls plasma cell function through the regulation of immunoglobulin secretion and the unfolded protein response. *Nat Immunol* **17**, 323-330 (2016).
50. Godfrey, L. et al. DOT1L inhibition reveals a distinct subset of enhancers dependent on H3K79 methylation. *Nat. Comm.* **10**, 2803-2803 (2019).
51. Huff, J.T., Plocik, A.M., Guthrie, C. & Yamamoto, K.R. Reciprocal intronic and exonic histone modification regions in humans. *Nat. Struct. Mol. Biol.* **17**, 1495-1499 (2010).
52. Cano-Rodriguez, D. et al. Writing of H3K4Me3 overcomes epigenetic silencing in a sustained but context-dependent manner. *Nat Commun* **7**, 12284 (2016).
53. Schubeler, D. et al. The histone modification pattern of active genes revealed through genome-wide chromatin analysis of a higher eukaryote. *Genes Dev.* **18**, 1263-1271 (2004).
54. Wang, Z. et al. Combinatorial patterns of histone acetylations and methylations in the human genome. *Nat. Genet.* **40**, 897-903 (2008).
55. Yang, A. et al. A chemical biology route to site-specific authentic protein modifications. *Science* **354**, 623-626 (2016).
56. Cecere, G., Hoersch, S., Jensen, M.B., Dixit, S. & Grishok, A. The ZFP-1(AF10)/DOT-1 complex opposes H2B ubiquitination to reduce Pol II transcription. *Mol. Cell* **50**, 894-907 (2013).
57. Xiao, Z., Chen, L., Zhou, Q. & Zhang, W. Dot1l deficiency leads to increased intercalated cells and upregulation of V-ATPase B1 in mice. *Exp. Cell Res.* **344**, 167-175 (2016).
58. Zhang, W. et al. Aldosterone-sensitive repression of ENaCalpha transcription by a histone H3 lysine-79 methyltransferase. *Am J Physiol. Cell. Physiol.* **290**, C936-946 (2006).
59. Zhang, W., Xia, X., Reisenauer, M.R., Hemenway, C.S. & Kone, B.C. Dot1a-AF9 complex mediates histone H3 Lys-79 hypermethylation and repression of ENaCalpha in an aldosterone-sensitive manner. *J. Biol. Chem.* **281**, 18059-18068 (2006).
60. Su, I.H. et al. Ezh2 controls B cell development through histone H3 methylation and Igh rearrangement. *Nat Immunol* **4**, 124-131 (2003).

bioRxiv preprint doi: https://doi.org/10.1101/826370; this version posted November 18, 2019. The copyright holder for this preprint (which was not certified by peer review) is the author/funder, who has granted bioRxiv a license to display the preprint in perpetuity. It is made available under aCC-BY-NC-ND 4.0 International license.

61. Guo, M. et al. EZH2 Represses the B Cell Transcriptional Program and Regulates Antibody-Secreting Cell Metabolism and Antibody Production. *J Immunol* **200**, 1039-1052 (2018).
62. Beguelin, W. et al. EZH2 enables germinal centre formation through epigenetic silencing of CDKN1A and an Rb-E2F1 feedback loop. *Nat Commun* **8**, 877 (2017).
63. Caganova, M. et al. Germinal center dysregulation by histone methyltransferase EZH2 promotes lymphomagenesis. *J. Clin. Invest.* **123**, 5009-5022 (2013).
64. Fan, T. et al. EZH2-dependent suppression of a cellular senescence phenotype in melanoma cells by inhibition of p21/CDKN1A expression. *Mol Cancer Res* **9**, 418-429 (2011).
65. Sato, T. et al. PRC2 overexpression and PRC2-target gene repression relating to poorer prognosis in small cell lung cancer. *Sci Rep* **3**, 1911 (2013).
66. Frangini, A. et al. The aurora B kinase and the polycomb protein ring1B combine to regulate active promoters in quiescent lymphocytes. *Mol. Cell* **51**, 647-661 (2013).
67. Rajewsky, K. Clonal selection and learning in the antibody system. *Nature* **381**, 751-758 (1996).
68. LeBien, T.W. & Tedder, T.F. B lymphocytes: how they develop and function. *Blood* **112**, 1570-1580 (2008).
69. Busslinger, M. & Tarakhovsky, A. Epigenetic control of immunity. *Cold Spring Harb Perspect Biol* **6** (2014).
70. Bao, Y. & Cao, X. Epigenetic Control of B Cell Development and B-Cell-Related Immune Disorders. *Clin Rev Allergy Immunol* **50**, 301-311 (2016).
71. Parra, M. Epigenetic events during B lymphocyte development. *Epigenetics* **4**, 462-468 (2009).
72. Ishiguro, K. et al. DOT1L inhibition blocks multiple myeloma cell proliferation by suppressing IRF4-MYC signaling. *Haematologica* **104**, 155-165 (2019).
73. Deshpande, A. et al. Targeting MYC-Driven B-Cell Lymphoma By Inhibition of the Histone Methyltransferase DOT1L. *Blood* **132**, 2839 (2018).
74. Wong, M. et al. The Histone Methyltransferase DOT1L Promotes Neuroblastoma by Regulating Gene Transcription. *Cancer Res.* **77**, 2522-2533 (2017).
75. Bodega, B. et al. A cytosolic Ezh1 isoform modulates a PRC2–Ezh1 epigenetic adaptive response in postmitotic cells. *Nat. Struct. Mol. Biol.* **24**, 444-452 (2017).
76. Choi, J. et al. DNA binding by PHF1 prolongs PRC2 residence time on chromatin and thereby promotes H3K27 methylation. *Nat. Struct. Mol. Biol.* **24**, 1039-1047 (2017).
77. Dobenecker, M.W. et al. Signaling function of PRC2 is essential for TCR-driven T cell responses. *J Exp Med* **215**, 1101-1113 (2018).
78. Jani, K.S. et al. Histone H3 tail binds a unique sensing pocket in EZH2 to activate the PRC2 methyltransferase. *Proc. Natl. Acad. Sci. U.S.A.* **116**, 8295-8300 (2019).
79. Ji, Y. et al. miR-155 harnesses Phf19 to potentiate cancer immunotherapy through epigenetic reprogramming of CD8 + T cell fate. *Nat. Comm.* (2019).
80. Lee, C.-H. et al. Distinct Stimulatory Mechanisms Regulate the Catalytic Activity of Polycomb Repressive Complex 2. *Mol. Cell* **70**, 435-448.e435 (2018).
81. Lee, C.-H. et al. Allosteric activation dictates PRC2 activity independent of its recruitment to chromatin. *Mol. Cell* **70**, 422-422 (2018).
82. Moritz, L.E. & Trievel, R.C. Structure, mechanism, and regulation of polycomb-repressive complex 2. *J. Biol. Chem.* **293**, 13805-13814 (2018).
83. Sanulli, S. et al. Jarid2 Methylation via the PRC2 Complex Regulates H3K27me3 Deposition during Cell Differentiation. *Mol. Cell* **57**, 769-769 (2015).
84. Healy, E. et al. PRC2.1 and PRC2.2 Synergize to Coordinate H3K27 Trimethylation. *Mol. Cell* (2019).
85. van Mierlo, G., Veenstra, G.J.C., Vermeulen, M. & Marks, H. The Complexity of PRC2 Subcomplexes. *Trends Cell Biol.* **29**, 660-671 (2019).
86. Su, I.h. et al. Polycomb Group Protein Ezh2 Controls Actin Polymerization and Cell Signaling. *Cell* **121**, 425-436 (2005).
87. Hobeika, E. et al. Testing gene function early in the B cell lineage in mb1-cre mice. *Proc. Natl. Acad. Sci. U.S.A.* **103**, 13789-13794 (2006).
88. McCarthy, D.J., Chen, Y. & Smyth, G.K. Differential expression analysis of multifactor RNA-Seq experiments with respect to biological variation. *Nucl. Acids Res.* **40**, 4288-4297 (2012).
89. Robinson, M.D., McCarthy, D.J. & Smyth, G.K. edgeR: a Bioconductor package for differential expression analysis of digital gene expression data. *Bioinformatics* **26**, 139-140 (2010).
90. Wu, D. et al. ROAST: rotation gene set tests for complex microarray experiments. *Bioinformatics* **26**, 2176-2182 (2010).

bioRxiv preprint doi: https://doi.org/10.1101/826370; this version posted November 18, 2019. The copyright holder for this preprint (which was not certified by peer review) is the author/funder, who has granted bioRxiv a license to display the preprint in perpetuity. It is made available under aCC-BY-NC-ND 4.0 International license.

Figure legends

Figure 1: Expression levels, efficient deletion of Dot1L in B cells and its effect on cellularity of B lineage subsets in the bone marrow.

a) Expression of Dot1L in different B-cell populations [37]. B1: B1 cells, MZB: Marginal Zone B, FOB: Follicular B, GCB: Germinal Center B, SPLPB: spleen plasma blast, SPLPC: spleen plasma cells and Bone Marrow (BMPC: Bone marrow plasma cells). Expression is shown as transcript per million (TPM). Note, SPLPB and BMPC lack SD as replicates were lacking. b) Intracellular flow-cytometry staining for H3K79me2 in bone marrow B-cell subsets as well as splenic B and T cells from *MB1Cre;Dot1L*$^{wt/wt}$ (WT) and *MB1Cre;Dot1L*$^{fl/fl}$ (KO) mice. Results represent the data from two independent experiments. c) Absolute number of total nucleated cells from bone marrow B-cell subsets; p-value from Student t-test is indicated.

Figure 2: Dot1L ablation affects the cellularity of mature peripheral B cell populations with a strong reduction in Marginal Zone and Germinal Center B cells.

(a-h) Absolute number of total nucleated splenocytes, splenic B-and T cells and indicated mature B cell subsets in *MB1Cre;Dot1L*$^{wt/wt}$ (WT) and *MB1Cre;Dot1L*$^{fl/fl}$ (KO) mice; p-value from Student t-test is indicated. Error bars indicate mean with range. (i) Number of germinal center B cells (PNA^{high}, CD95^{+}) and their flow cytometric analysis from the spleen of unchallenged WT and KO mice; p-value from t-test is indicated. Error bars indicate mean ±SD (j and k). The quantification and identification of germinal centers lectin histochemistry of Peanut agglutinin (PNA) in spleens from WT and KO mice. The scale bar: 20 μm. Error bars indicate mean with ±SD.

Figure 3: DOT1L is essential for efficient CSR and proliferation.

(a-b) Analysis of DOT1L-proficient (WT) and DOT1L-deficient (KO) naïve B cells activated for four days with LPS alone (IgG3 switching) or with LPS and IL-4 (IgG1 switching); p-value from Student t-test is indicated. Error bars indicate mean ±SD. c) Analysis of DOT1L-proficient (WT) and -deficient (KO) B cells, activated for four days with anti-CD40 and IL-4 (IgG1 switching) B cells. The graph indicates the statistical analysis (Student t test) of the percentages of B cells that switched to IgG1 in WT and KO; p-value from t-test is indicated. Error bars indicate

bioRxiv preprint doi: https://doi.org/10.1101/826370; this version posted November 18, 2019. The copyright holder for this preprint (which was not certified by peer review) is the author/funder, who has granted bioRxiv a license to display the preprint in perpetuity. It is made available under aCC-BY-NC-ND 4.0 International license.

mean ±SD. d) Naïve B cells were labeled with cell trace violet (CTV) and stimulated for four days with anti-CD40 and IL-4. CTV dilution was measured by flow cytometry. Results from three independent WT and KO mice are depicted.

Figure 4: DOT1L-deficient B cells fail to mount an efficient immune response but show signs of plasma-cell differentiation upon challenge.

a) Representative flow cytometry plots of splenic GC B cells 14 days after LCMV Armstrong infection in WT and Dot1L-KO mice and their statistical analyses. Error bars indicate mean with ±SD. b Representative flow cytometry plots of plasma cells B from the spleen at 14 days after LCMV infection and their statistical analyses. Error bars indicate mean with ±SD. c) LCMV-specific IgM and IgG titers in the serum of WT and KO mice before (D0) and 14 days after (D14) infection; number indicates p-value of a Student t-test. Error bars indicate mean with ±SD. d) WT and KO mice were challenged with the model antigen 4-hydroxy-3-nitrophenylacetyl conjugated to chicken gamma globulin (NP-CGG). NP-specific IgG1 and IgM titers were quantified by ELISA from the serum isolated at the indicated days following immune challenge. Error bars indicate mean with ± standard error of mean (SEM).

Figure 5: Transcriptome analysis of in-vitro activated B cells shows accelerated plasma-cell differentiation and compromised activation of MYC-target genes in the absence of DOT1L.

a) MA-Plot of normalized RNA-Seq data showing differentially expressed genes (FDR < 0.05) between Dot1L-KO and WT B cells after two days of in vitro activation with LPS+IL-4. b Differential expression of Bach2, Prdm1 (encoding BLIMP-1), CD138 and Myc transcripts are indicated as CPM after TMM normalization from WT and KO. Error bars indicate mean ±SD. c) BARCODE plot showing the enrichment of plasma-cell signature genes in KO as compared to WT activated B cells. d) BARCODE plot showing the enrichment of MYC-target genes in WT as compared to KO activated B cells. p values showing the statistical significance of enrichment of gene set calculated via FRY test are indicated.

Figure 6: DOT1L-mediated H3K79 methylation is associated with gene activity in B cells and indirectly promotes repression of PRC2 target genes.

bioRxiv preprint doi: https://doi.org/10.1101/826370; this version posted November 18, 2019. The copyright holder for this preprint (which was not certified by peer review) is the author/funder, who has granted bioRxiv a license to display the preprint in perpetuity. It is made available under aCC-BY-NC-ND 4.0 International license.

a) Integrative analyses of differentially expressed transcripts (FDR < 0.05) from activated and naïve Dot1L-deficient B cells (left panel) with H3K79me2 ChIP values from WT activated and naïve B cells (right panel). b) The distribution of mean H3K79me2 amongst different gene sets from activated and naïve B cells as depicted by box-plots. c) Differential expression of *Ezh2* and *Cdkn1a* is depicted as CPM after TMM normalization from WT and Dot1L-KO activated B cells. Error bars indicate mean ±SD. d) H3K79me2 methylation at the Ezh2 locus from WT activated and naïve B cells, as determined by reads per genomic content (RPGC); three independent replicates are shown. e) Scatter plot showing the correlation between expression of Ezh2 and Dot1L as depicted in TPM in different mature B-cell subsets; B1: B1 cells, MZB: Marginal Zone B, FOB: Follicular B, GCB: Germinal Center B, SPLPB: spleen plasma blast, SPLPC: spleen plasma cells) and Bone Marrow (BMPC: Bone marrow plasma cells) A20: Germinal Center like cell lymphoma cell line. f) Coverage plot of H3K27me3 from naïve B cells [66] and H3K79me2 (from WT naïve and activated B cells) flanking four kb around transcriptional start sites (TSS) for genes upregulated in KO (KO Gain) or non-differential Expression Matched genes is shown. Coverage was calculated as reads per genomic content cutoff at the 0.995th quantile and rescaled to a maximum of 1.

bioRxiv preprint doi: https://doi.org/10.1101/826370; this version posted November 18, 2019. The copyright holder for this preprint (which was not certified by peer review) is the author/funder, who has granted bioRxiv a license to display the preprint in perpetuity. It is made available under aCC-BY-NC-ND 4.0 International license.

Table 1: Ingenuity Pathway Analysis of upstream transcriptional regulators that are differentially expressed in WT versus *Dot1L* knock-out naïve B cells (FDR < 0.05)

Upstream Transcriptional Regulator	Expression Log Ratio (KO/WT)	Activation z-score	p-value of overlap
HIF1A	-1.534	5.138	3.22E-10
EZH2	-1.195	0.27	1.33E-04
REL	-1.146	1.685	9.25E-05
TAF4B	-1.042		3.96E-02
IRF4	-1.038	-3.202	1.93E-03
MED13	-0.978	-2.143	6.70E-03
SIRT1	-0.973	-3.106	7.11E-09
PURA	-0.964	1.067	2.23E-03
EBF1	-0.95	2.612	7.55E-08

bioRxiv preprint doi: https://doi.org/10.1101/826370; this version posted November 18, 2019. The copyright holder for this preprint (which was not certified by peer review) is the author/funder, who has granted bioRxiv a license to display the preprint in perpetuity. It is made available under aCC-BY-NC-ND 4.0 International license.

Table 2: Surface markers for identification of specific cellular population

Bone Marrow

B cells	$CD19^{+}B220^{+}$
Immature B cells	$CD19^{+}B220^{low}IgM^{+}$
Mature B cells	$CD19^{+}B220^{high}IgM^{+}$
Pro B cells	$CD19^{+}B220^{low}IgM^{-}c\text{-}Kit^{+}CD25^{-}$
Pre B cells	$CD19^{+}B220^{low}IgM^{-}c\text{-}Kit^{-}CD25^{+}$

Spleen

B cells	$CD19^{+}B220^{+}$
B1-a cells	$CD19^{+}B220^{low}$
T1 cells	$CD19^{+}B220^{+}CD23^{-/low}CD21/35^{-/low}IgM^{high}$
T2 cells	$CD19^{+}B220^{+}CD23^{high}CD21/35^{-/low}IgM^{high}$
Marginal Zone progenitor	$CD19^{+}B220^{+}CD23^{high}CD21/35^{high}IgM^{high}$
Marginal Zone B cells	$CD19^{+}B220^{+}CD23^{-/low}CD21/35^{high}IgM^{high}$
Follicular B cells	$CD19^{+}B220^{+}CD23^{high}CD21/35^{low}IgM^{-/low}$
Follicular B-I cells	$B220^{+}CD93^{-/low}CD21/35^{low}IgM^{low}IgD^{high}$
Follicular B-II cells	$B220^{+}CD93\text{-}CD21/35^{low}IgM^{high}IgD^{high}$
Germinal center B cells	$CD19^{+}B220^{+}PNA/GL7^{high}CD95^{high}$
Plasma cells	$CD19^{+}B220^{+}IgD\text{-}CD138^{+}$
T cells	$CD3^{+}CD19^{-}$

Peyer's patches

Germinal center B cells	$CD19^{+}B220^{+}PNA/GL7^{high}CD95^{high}$

bioRxiv preprint doi: https://doi.org/10.1101/826370; this version posted November 18, 2019. The copyright holder for this preprint (which was not certified by peer review) is the author/funder, who has granted bioRxiv a license to display the preprint in perpetuity. It is made available under aCC-BY-NC-ND 4.0 International license.

Table 3: Antibodies used for flowcytometry

Bone Marrow

Antibodies	Flourophore	Clone	Dilution	Vendor
CD19	APC-H7	1D3	1:200	BD Pharmingen
CD19	PerCpCy5,5	1D3	1:200	BD Pharmingen
CD45R (B220)	Pacific Blue	RA3-6B2	1:200	BD Pharmingen
IgM	PECy7	11/41	1:200	eBioscience
CD117 (cKit)	APC	2B8	1:200	eBioscience
CD25	PE	PC61	1:200	Biolegend
IgD	FITC	11-26c.2a	1:200	BD Pharmingen
DAPI			1:20	Sigma-Aldrich
PI			1:20	Sigma-Aldrich

Spleen

Antibodies	Flourophore	Clone	Dilution	Vendor
Gl-7	FITC	GL7	1:200	BD Pharmingen
Peanut Agglutinin	FITC		1:400	Vector
CD23	BV421	B3B4	1:200	Biolegend
CD19	PerCpCy5,5	1D3	1:200	BD Pharmingen
CD19	APC-H7	1D3	1:200	BD Pharmingen
CD19	A780	1D3	1:200	eBioscience
CD95	Biotin	15A7	1:100	eBioscience
CD95	PE	Jo2	1:200	BD Pharmingen
CD21/35	APC	7E9	1:200	Biolegend
CD93	BV650	AA4.1	1:200	BD Pharmingen
IgM	BV785	II/41	1:200	BD Pharmingen

bioRxiv preprint doi: https://doi.org/10.1101/826370; this version posted November 18, 2019. The copyright holder for this preprint (which was not certified by peer review) is the author/funder, who has granted bioRxiv a license to display the preprint in perpetuity. It is made available under aCC-BY-NC-ND 4.0 International license.

IgD	BV650	11-26c.2a	1:200	Biolegend
IgD	PE	11-26C	1:800	eBioscience
IgD	AF-488	11-26c2a	1:200	eBioscience
CD3	FITC	17A2	1:200	Biolegend
CD3	AF488	145-2C11	1:200	eBioscience
CD45R (B220)	V500	RA3-6B2	1:200	BD Pharmingen
CD45R (B220)	PB	RA3-6B2	1:200	BD Pharmingen
CD45R (B220)	APC	RA3-6B2	1:200	BD Pharmingen
CD45R (B220)	BV510	RA3-6B2	1:200	Biolegend
CD138	PE	281-2	1:200	BD Pharmingen
CD138	BV605	281-2	1:200	Biolegend
Strepavidin	BV605		1:400	BD Pharmingen
Zombie NIR			1:1000	Biolegend
7AAD			1:500	Biolegend
PI			1:20	Sigma-Aldrich
DAPI			1:20	Sigma-Aldrich

Peyer's Patches

Antibodies	Flourophore	Clone	Dilution	Vendor
CD45R (B220)	Pacific Blue	RA3-6B2	1:200	BD Pharmingen
CD19	PerCpCy5,5	1D3	1:200	BD Pharmingen
IgM	APC	Polyclonal	1:200	Southern Biotech
Peanut Agglutinin	FITC		1:400	Vector
CD95	PE	Jo2	1:200	BD Pharmingen
DAPI			1:20	Sigma-Aldrich

bioRxiv preprint doi: https://doi.org/10.1101/826370; this version posted November 18, 2019. The copyright holder for this preprint (which was not certified by peer review) is the author/funder, who has granted bioRxiv a license to display the preprint in perpetuity. It is made available under aCC-BY-NC-ND 4.0 International license.

Class switch recombination (*In vitro*)

Antibodies	Flourophore	Clone	Dilution	Vendor
CD19	PerCpCy5,5	1D3	1:400	BD Pharmingen
IgG1	PE	15H6	1:800	Southern Biotech
IgM	APC	Polyclonal	1:1000	Southern Biotech
IgG3	PE	Polyclonal	1:800	Southern Biotech
DAPI			1:20	Sigma-Aldrich

Plasma cells (*In vitro*)

Antibodies	Flourophore	Clone	Dilution	Vendor
CD138	BV605	281-2	1:200	Biolegend
CD45R (B220)	BV510	RA3-6B2	1:200	Biolegend
IgD	BV650	11-26c.2a	1:200	Biolegend
Sca1	PeCy7	D7	1:200	Biolegend
CD3e	APC	145-2C11	1:200	BD Pharmingen
Ter119	APC	TER-119	1:200	BD Pharmingen
Blimp*	PE	SE7	1:200	Biolegend
Zombie NIR			1:1000	Biolegend
* Intracellular				

bioRxiv preprint doi: https://doi.org/10.1101/826370; this version posted November 18, 2019. The copyright holder for this preprint (which was not certified by peer review) is the author/funder, who has granted bioRxiv a license to display the preprint in perpetuity. It is made available under aCC-BY-NC-ND 4.0 International license.

Fig. 1

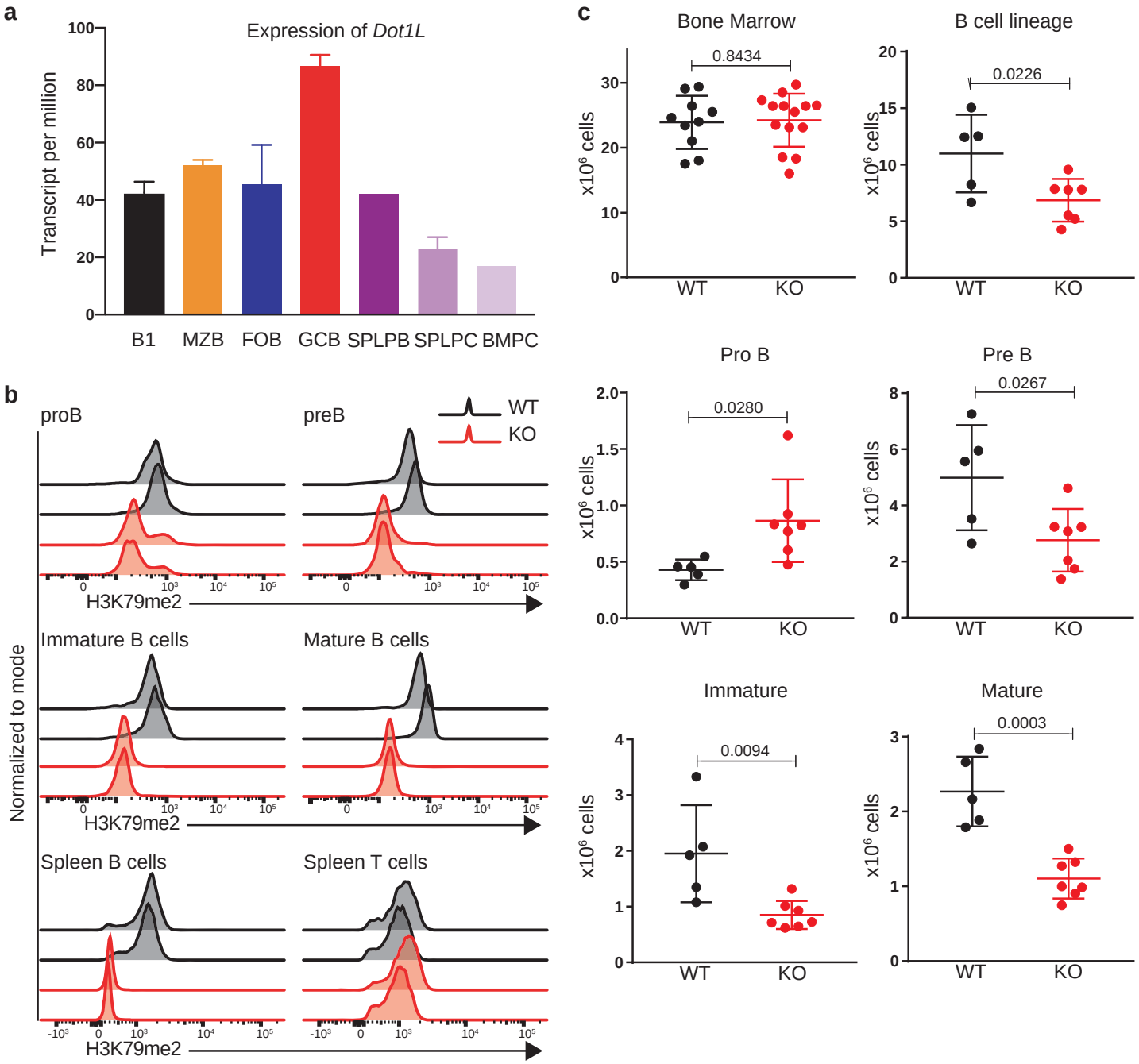

bioRxiv preprint doi: https://doi.org/10.1101/826370; this version posted November 18, 2019. The copyright holder for this preprint (which was not certified by peer review) is the author/funder, who has granted bioRxiv a license to display the preprint in perpetuity. It is made available under aCC-BY-NC-ND 4.0 International license.

Fig. 2

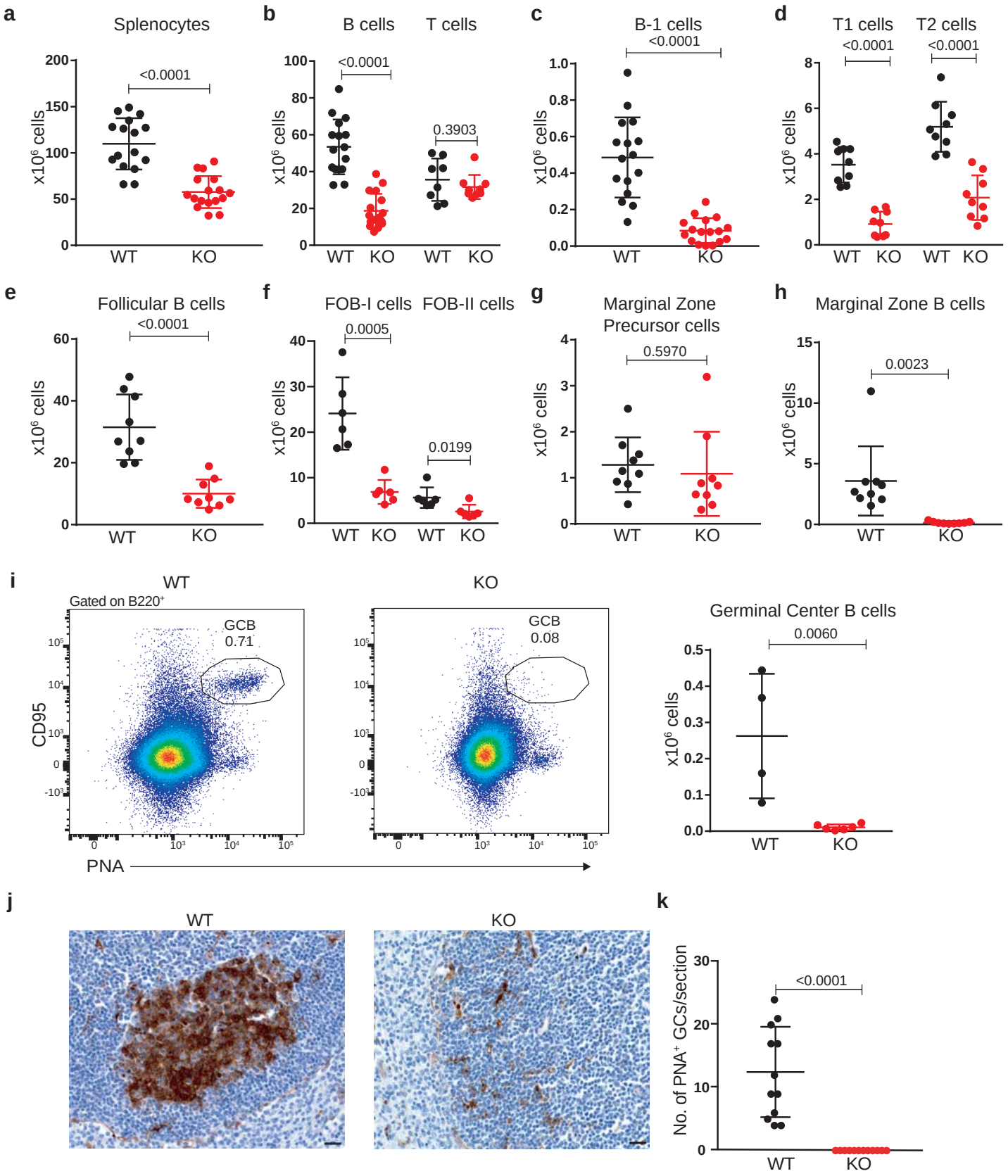

bioRxiv preprint doi: https://doi.org/10.1101/826370; this version posted November 18, 2019. The copyright holder for this preprint (which was not certified by peer review) is the author/funder, who has granted bioRxiv a license to display the preprint in perpetuity. It is made available under aCC-BY-NC-ND 4.0 International license.

Fig. 3

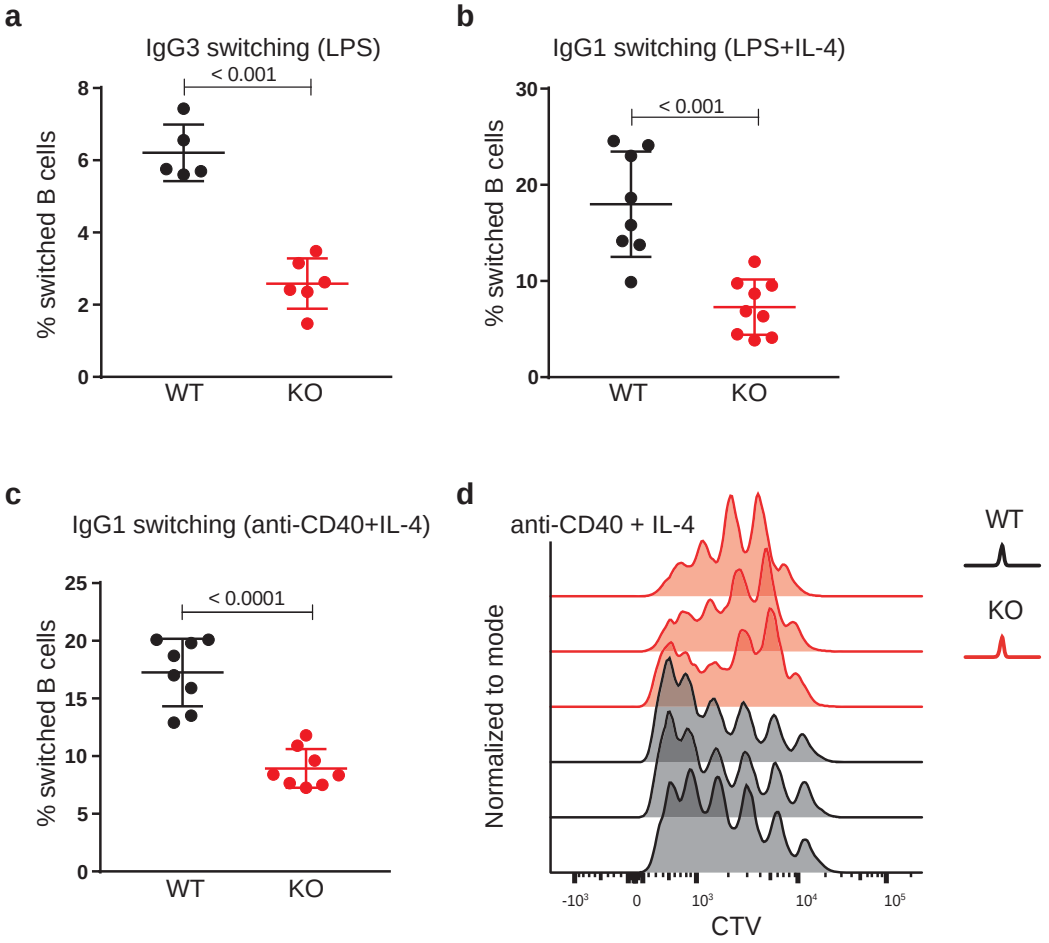

bioRxiv preprint doi: https://doi.org/10.1101/826370; this version posted November 18, 2019. The copyright holder for this preprint (which was not certified by peer review) is the author/funder, who has granted bioRxiv a license to display the preprint in perpetuity. It is made available under aCC-BY-NC-ND 4.0 International license.

Fig. 4

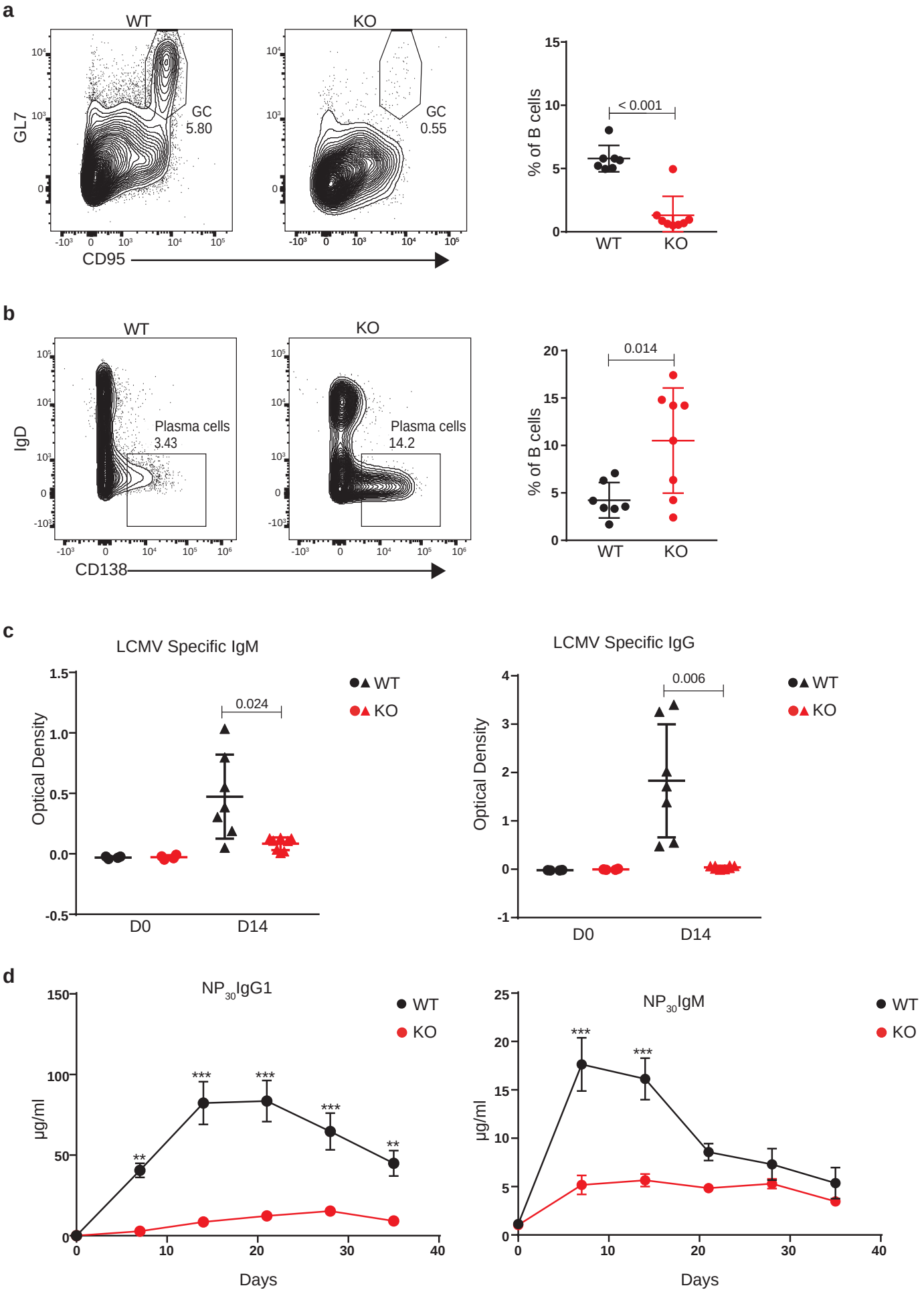

bioRxiv preprint doi: https://doi.org/10.1101/826370; this version posted November 18, 2019. The copyright holder for this preprint (which was not certified by peer review) is the author/funder, who has granted bioRxiv a license to display the preprint in perpetuity. It is made available under aCC-BY-NC-ND 4.0 International license.

Fig. 3

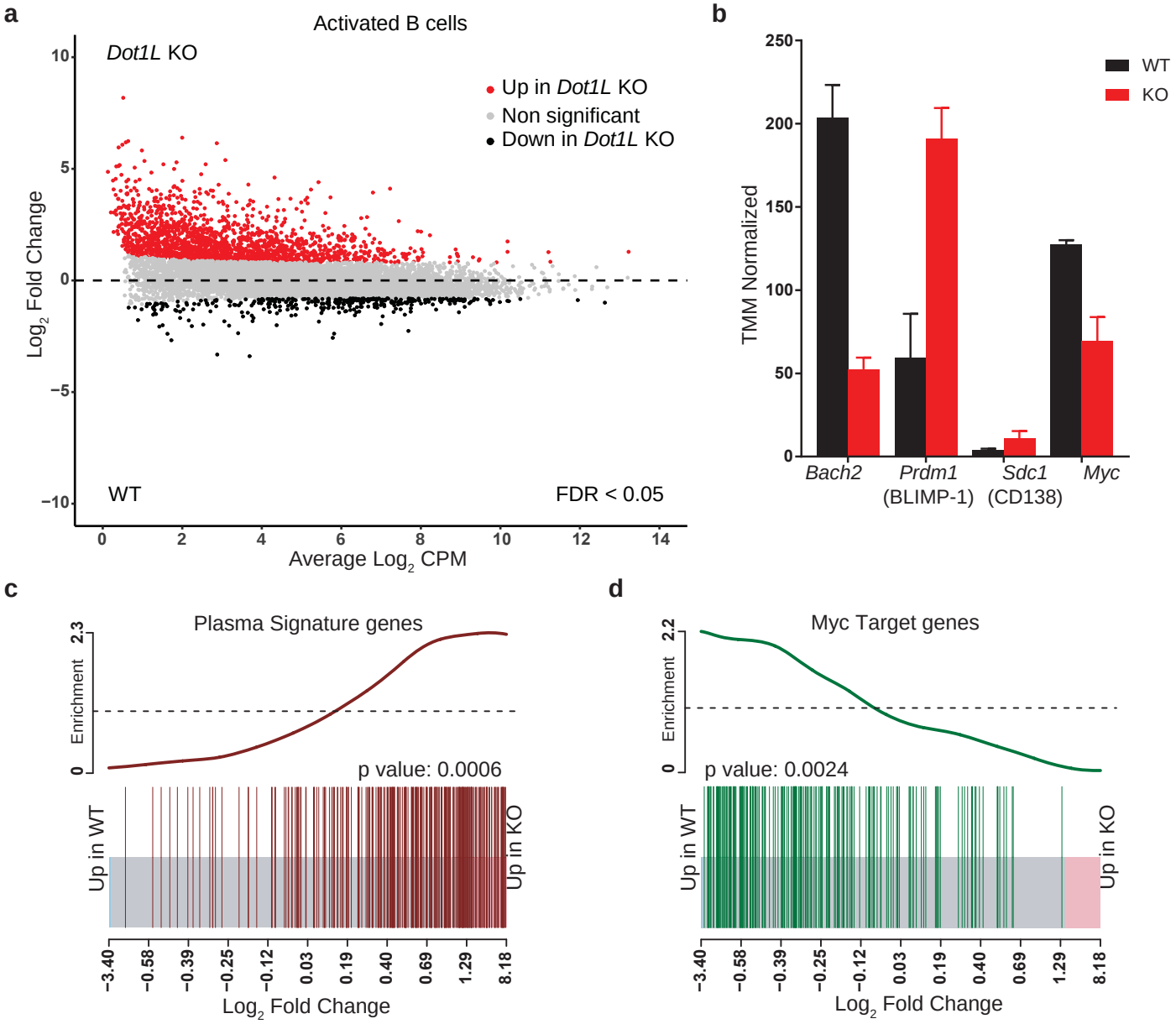

bioRxiv preprint doi: https://doi.org/10.1101/826370; this version posted November 18, 2019. The copyright holder for this preprint (which was not certified by peer review) is the author/funder, who has granted bioRxiv a license to display the preprint in perpetuity. It is made available under aCC-BY-NC-ND 4.0 International license.
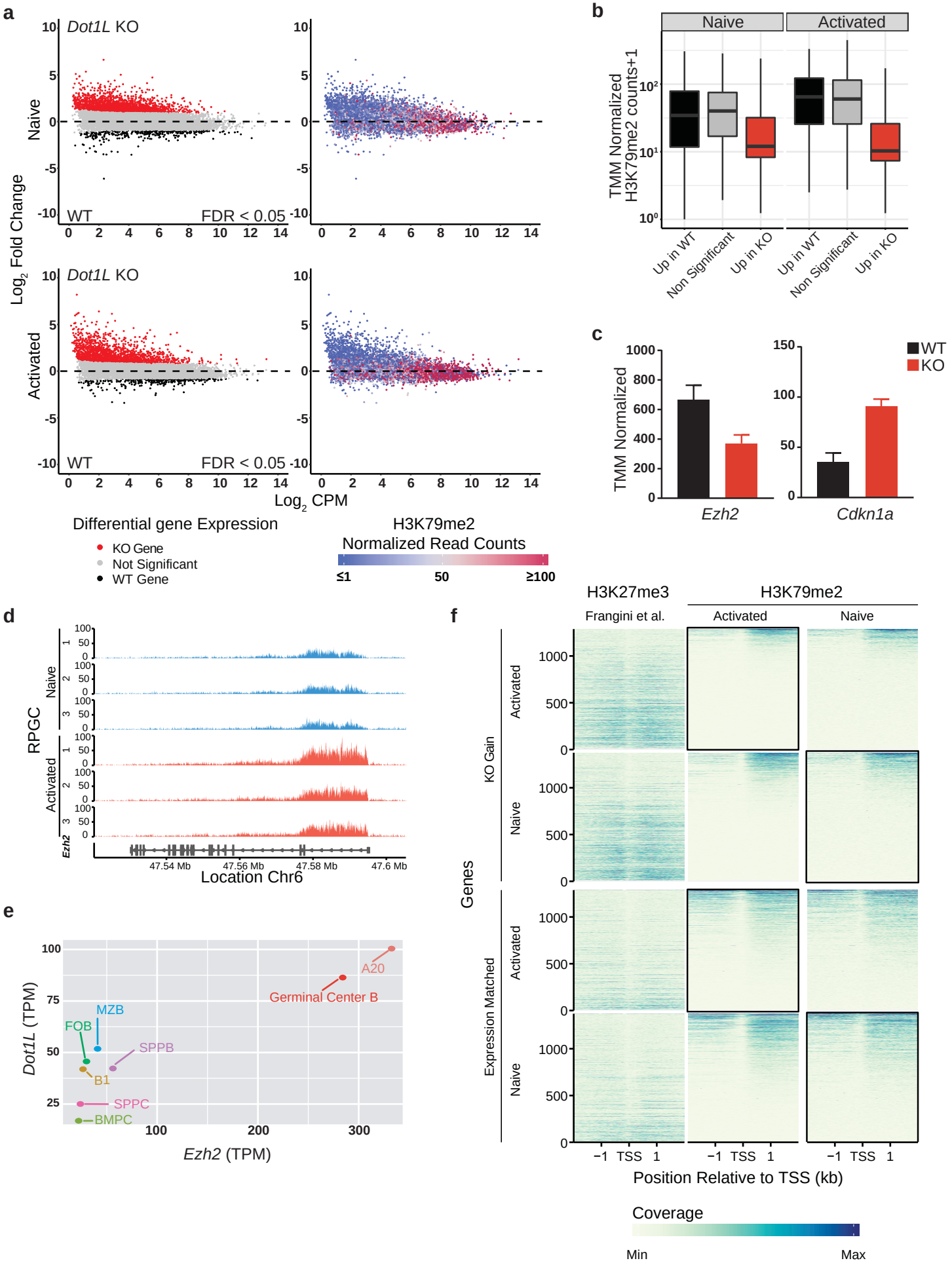
Fig. 6